7-26-2022

Thioester Synthesis By a Designed Nickel Enzyme Models Prebiotic Energy Conversion

A. C. Manesis

A. Yerbulekova

Jason M. Shearer
Trinity University, jshearer@trinity.edu

H. S. Shafaat

PNAS RESEARCH ARTICLE | CHEMISTRY BIOCHEMISTRY

Thioester synthesis by a designed nickel enzyme models prebiotic energy conversion

Anastasia C. Manesis[a,1,2], Alina Yerbulekova[a,1], Jason Shearer[b], and Hannah S. Shafaat[a,c,3]

Edited by Marcetta Darensbourg, Texas A&M University, College Station, TX; received December 21, 2021; accepted April 12, 2022

The formation of carbon–carbon bonds from prebiotic precursors such as carbon dioxide represents the foundation of all primordial life processes. In extant organisms, this reaction is carried out by the carbon monoxide dehydrogenase (CODH)/acetyl coenzyme A synthase (ACS) enzyme, which performs the cornerstone reaction in the ancient Wood–Ljungdahl metabolic pathway to synthesize the key biological metabolite, acetyl-CoA. Despite its significance, a fundamental understanding of this transformation is lacking, hampering efforts to harness analogous chemistry. To address these knowledge gaps, we have designed an artificial metalloenzyme within the azurin protein scaffold as a structural, functional, and mechanistic model of ACS. We demonstrate the intermediacy of the Ni^{I} species and requirement for ordered substrate binding in the bioorganometallic carbon–carbon bond-forming reaction from the one-carbon ACS substrates. The electronic and geometric structures of the nickel-acetyl intermediate have been characterized using time-resolved optical, electron paramagnetic resonance, and X-ray absorption spectroscopy in conjunction with quantum chemical calculations. Moreover, we demonstrate that the nickel-acetyl species is chemically competent for selective acyl transfer upon thiol addition to biosynthesize an activated thioester. Drawing an analogy to the native enzyme, a mechanism for thioester generation by this ACS model has been proposed. The fundamental insight into the enzymatic process provided by this rudimentary ACS model has implications for the evolution of primitive ACS-like proteins. Ultimately, these findings offer strategies for development of highly active catalysts for sustainable generation of liquid fuels from one-carbon substrates, with potential for broad applications across diverse fields ranging from energy storage to environmental remediation.

bioorganometallic | acetyl coenzyme A synthase | metalloprotein design | carbon–carbon coupling | activated thioester

Significance

Acetyl coenzyme A synthase (ACS) is the cornerstone metalloenzyme in carbon fixation and energy conservation in primordial microorganisms and offers a roadmap for generating liquid fuels from carbon dioxide, but how ACS works remains debated. Here we gain insight into this process by constructing an artificial metalloenzyme that performs analogous chemistry. We demonstrate the intermediacy of the Ni^{I} species and ordered substrate binding in the bioorganometallic carbon–carbon bond-forming reaction. In addition, we characterize the nickel-acetyl species, which is competent for biochemical synthesis of an activated thioester. Beyond providing a framework for understanding the native enzymatic mechanism, this work provides design guidelines for synthetic catalysts that harness these chemical principles and offers insight into the evolution of prebiotic energy conversion processes.

Current origins of life theories support a chemoautotrophic process by which carbon became assimilated into cellular biomass through the reductive acetyl-CoA, or Wood–Ljungdahl (WL), pathway (1, 2). This metabolic process fixes carbon dioxide using hydrogen as an energy source and is thought to link the abiotic Earth with the emergence of microbial life, as the WL pathway is the only carbon fixation process identified in the last universal common ancestor, the ancient microorganism from which both bacteria and archaea (and subsequently eukaryotes) evolved (3, 4). Consistent with this hypothesis, modern organisms that rely on the WL pathway inhabit primordial environments rich in simple small molecules such as CO_2, H_2, and H_2S and reduced metals such as iron and nickel. The cornerstone enzyme in the WL pathway is the carbon monoxide dehydrogenase/acetyl coenzyme A synthase (CODH/ACS) complex (Fig. 1*A*) (5). This large enzyme system requires multiple canonical iron–sulfur ([4Fe-4S]) clusters for electron transfer along with two unique nickel–iron–containing active sites. The site-differentiated [Ni-4Fe-4S] cluster of CODH is responsible for reducing CO_2 to CO (Eq. **1**) (6), while the ACS active site contains two nickel centers bridged to a [4Fe-4S] cluster through a cysteine thiolate ligand (7). The latter active site is responsible for coupling the CODH-derived CO with a CO_2-derived methyl group ("CH_3"), which is transferred in a concerted, two-electron process from a cobalt corrinoid iron–sulfur (CoFeSP) enzyme. The acetyl group is then transferred to CoA for generation of the thioester acetyl-CoA (Eq. **2**), a key biological metabolite.

$$CO_2 + 2H^+ + 2e^- \rightleftharpoons CO + H_2O \quad [1]$$

$$CO + Co^{III} - CH_3 + CoASH \rightleftharpoons CH_3CO - SCoA + Co^{I} + H^+. \quad [2]$$

As thioesters such as acetyl-CoA are considered the principal mechanism for primordial energy storage and conversion (1), understanding how thioester synthesis is carried out

Author contributions: A.C.M., A.Y., and H.S.S. designed research; A.C.M., A.Y., and J.S. performed research; A.C.M., A.Y., J.S., and H.S.S. analyzed data; and A.C.M., J.S., and H.S.S. wrote the paper.

The authors declare no competing interest.

This article is a PNAS Direct Submission.

[1]A.C.M. and A.Y. contributed equally to this work.

[2]Present address: Departments of Molecular Biosciences and Chemistry, Northwestern University, Evanston, IL 60208.

[3]To whom correspondence may be addressed. Email: shafaat.1@osu.edu.

This article contains supporting information online at http://www.pnas.org/lookup/suppl/doi:10.1073/pnas.2123022119/-/DCSupplemental.

Published July 18, 2022.

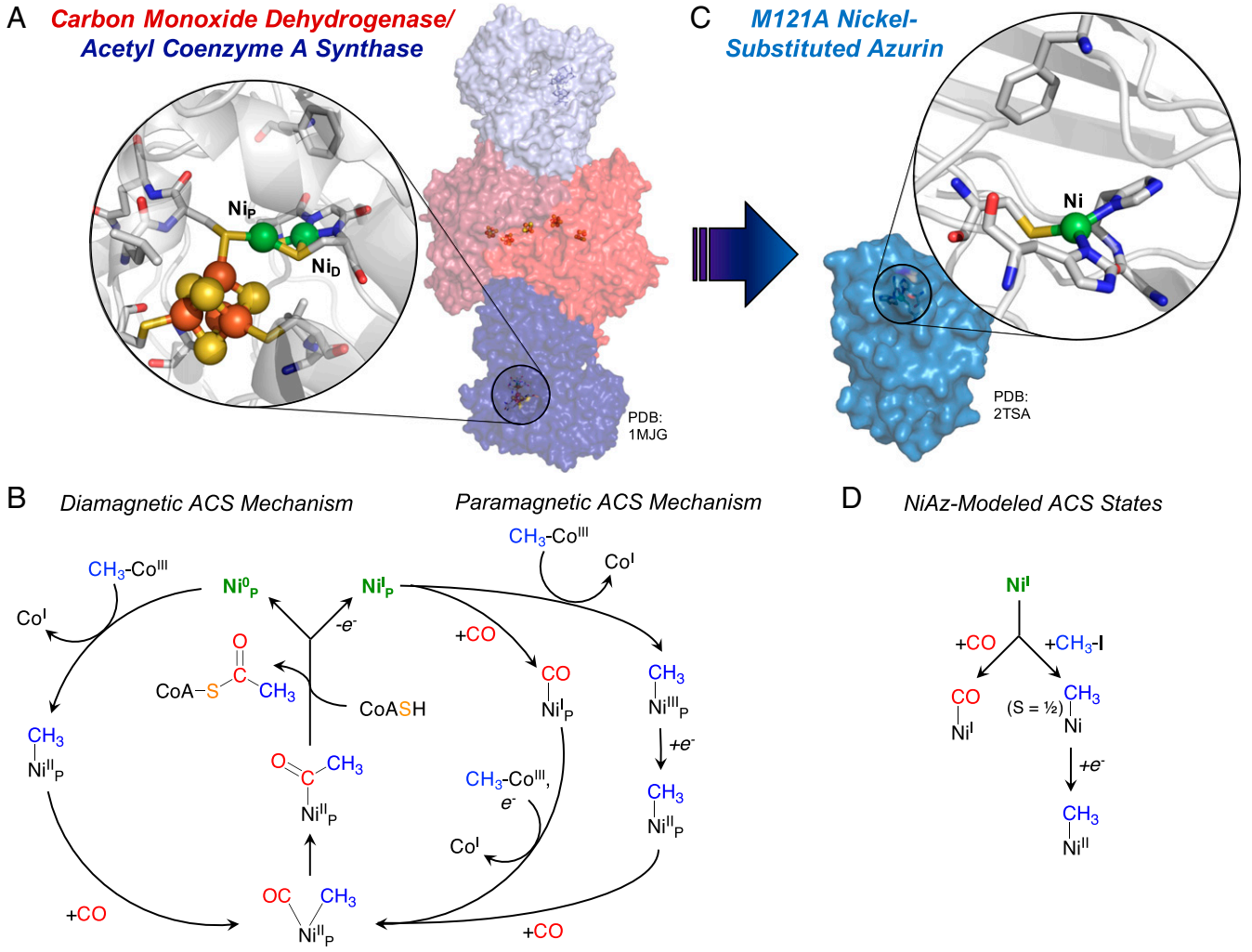

Fig. 1. Developing a protein-based model of acetyl coenzyme A synthase. The global protein and active site structures of (*A*) CODH/ACS and (*C*) M121A nickel-substituted azurin, with DFT geometry-optimized active site structure overlaid on the protein cartoon. (*B*) Proposed catalytic mechanisms for acetyl coenzyme A synthesis. (*D*) Models of catalytically relevant states of ACS previously characterized in M121A NiAz.

in nature represents an important stepping stone toward understanding premetabolic reactions.

However, many aspects of the ACS mechanism are fiercely debated by researchers in the field, including the relevant oxidation states, the metal centers involved in catalysis, and whether substrate binding is ordered or random. The current reigning models favor substrate conversion at only one nickel center (Fig. 1*B*), despite the presence of multiple metals in the active site. The "diamagnetic mechanism" invokes ordered substrate binding in which a cationic methyl group is first transferred to a Ni^0 center, giving a Ni^{II}–CH_3 species (8, 9). Carbon monoxide binding induces methyl migration (or CO insertion) to form a Ni^{II}-acetyl species, which is reductively thiolyzed by CoA to regenerate the Ni^0 species (10). The "paramagnetic mechanism" is associated with random substrate binding, in which either CO or a cationic methyl group can bind first to a Ni^I center (11). The absence of a formal Ni^{III} species in ACS has led to the proposal of an internal electron shuttle, which could rapidly reduce the transient formal Ni^{III}–CH_3 state, and acetyl formation and transfer to CoA are considered to occur from the Ni^{II} oxidation states. Thiolysis both regenerates the catalytic Ni^I state and reduces the internal electron shuttle (12). Several lines of experimental and computational evidence, some contradictory, exist to both corroborate and refute each mechanism (8, 12–15), while studies of native CODH/ACS continue to be complicated by the enzyme's instability, sensitivity to oxygen, and challenges associated with effective overexpression. Contributing to this ambiguity, only the Ni^I–CO state (A_{red}-CO) of ACS has been well characterized through recent X-ray crystallography, X-ray absorption, and pulsed electron paramagnetic resonance (EPR) studies (16–18). The key alkyl- and acyl-bound bioorganometallic species, which likely mediate the reversible carbon–carbon bond–forming and cleavage reactions, have yet to be observed in ACS.

The synthesis of molecular compounds that mimic enzyme active sites has substantially advanced our understanding of the native systems by providing structural, spectroscopic, and reactivity metrics. Synthetic models of ACS have been shown to be capable of supporting thioester synthesis from the addition of CO and a thiol to a methyl-bound nickel(II) center (19–22), although these reactions diverge from the enzyme-catalyzed processes in three critical ways: 1) Methyl binding requires use of either a Grignard reactant or the physiologically questionable Ni^0 oxidation state; 2) dry organic solvents rather than an aqueous solvation environment are necessary, suggesting hydrolysis and/or protonolysis would be favored over the biological thiolytic process; and 3) acyl transfer occurs directly to a bound thiolate ligand, resulting in irreversible decomposition. The

ligand environment around the active site also necessarily differs, and, to date, the reactivity of Ni^{I} model compounds has been restricted to radical methyl addition processes, casting doubt over the relevance of this paramagnetic redox state in the enzymatic process (13, 20, 23).

To gain a better understanding of native ACS as well as advance our understanding of how such a system may have evolved out of a primordial environment, a model with greater biological fidelity would be highly beneficial. A protein-based model of ACS would feature a primary coordination sphere that has biologically relevant ligands, a well-defined, asymmetric secondary coordination environment, site isolation to prevent bimolecular reactivity, and access to aqueous reaction conditions, allowing a direct comparison to ACS. The development and characterization of model metalloproteins has been highly valuable for the study of other complex metalloenzymes, including cytochrome *c* oxidase, hydrogenase, hydroxylamine oxidase, and polysaccharide monooxygenase, revealing subtle structural elements responsible for modulating reactivity of both the model and the native systems (24–29). Here, we demonstrate that a nickel-substituted, active-site mutant (M121A) of *Pseudomonas aeruginosa* azurin (Az) is both a structural and functional mimic of ACS (NiAz), binding both one-carbon substrates, CO and CH_3I, generating a new carbon–carbon bond, and releasing acetic acid upon acid-induced hydrolysis (Eq. **3**).

$$CO + CH_3I + H_3O^+ \rightleftharpoons CH_3COOH + 2H^+ + I^-. \quad [3]$$

Importantly, addition of a simple thiolate to the reaction mixture with M121A NiAz results in high selectivity toward the formation of a thioester, directly mimicking the chemistry of native ACS and fundamentally generating a compound that can be used for biological energy storage (Eq. **4**).

$$CO + CH_3I + CH_3S^- \rightleftharpoons CH_3COSCH_3 + I^-. \quad [4]$$

Optical, EPR, and X-ray absorption spectroscopy along with density functional theory (DFT) calculations reveal the electronic structures of substrate-bound species that are chemically competent, as well as others that are inhibitory, with direct application toward understanding the roles of analogous species in native ACS.

The active site of ACS, called the "A-cluster," contains a bimetallic nickel center bridged to a [4Fe-4S] cluster through a cysteine thiolate ligand. Despite this complexity, studies on the native enzyme suggest that only the low-coordinate, central Ni_P site is involved in catalysis (17). To probe the hypothesis that these organometallic transformations can occur in a protein at a single metal center, a monometallic model was constructed (Fig. 1*C*). The metal-binding site was designed based on the criteria that it must bind to nickel, which is the biologically relevant metal in ACS, and feature a coordination environment that resembles the Ni_P center, with ligands of comparable electronic structure in a pseudotrigonal geometry. Az, a naturally occurring cupredoxin, was selected as the protein scaffold, due to the small size of the system, structural robustness, and metal-binding promiscuity. The coordination sphere is dominated by one highly covalent thiolate ligand along with two strongly bound histidine ligands in a pseudotrigonal planar geometry, with weak axial interactions to a backbone carbonyl and the methionine-121 residue (30). Furthermore, prior studies on Az have indicated that the M121A mutation enables small molecules such as methanol and cyanide to access the Cu active site, offering a potential substrate binding channel (31).

Results

Nucleophilic Methyl Transfer from the Biochemically Competent Methylcobinamide Donor to Nickel Azurin Occurs Reversibly. Preparation of the nickel(II)-substituted M121A azurin (NiAz) mutant was carried out using standard techniques (32). Reduction of $Ni^{II}Az$ with $Eu^{II}DTPA$ results in quantitative conversion to M121A $Ni^{I}Az$ (Fig. 1*D*) (33). Spectroscopic and structural characterization of M121A $Ni^{I}Az$ reveals a trigonal planar active site bearing a close resemblance to the proposed A_{red}* state in ACS, which suggests that, from an electronic structure standpoint, the bridging thiolate ligands may be supplanted by histidine residues (34, 35). Exposure of M121A $Ni^{I}Az$ to CO results in a stable, four-coordinate Ni^{I}–CO species (32), while addition of CH_3I to M121A $Ni^{I}Az$ in the absence of residual reductant results in the formation of an S = 1/2 Ni–CH_3 species (33). Using pulsed EPR spectroscopy coupled with electronic structure analysis, the S = 1/2 Ni–CH_3 state was suggested to utilize an inverted ligand field (36, 37). In this case, the Ni center features a d^9 configuration, rather than a conventional d^7, Ni^{III} oxidation state, and the lowest unoccupied molecular orbital (LUMO) is centered on the electrophilic, cationic methyl ligand. The presence of inverted ligand fields within a model bioorganometallic system may serve as a means by which the protein can avoid degradative side reactions, including protonolysis or reductive elimination to methylate the bound cysteine residue (38–40). A similar electronic structure has thus been suggested for the analogous S = 1/2 Ni–CH_3 state in native ACS. This species continues to evade observation but is obligatory based on the optical signatures of the cobalt corrinoid methylating protein (CoFeSP), which converts directly from a Co^{III}–CH_3 state to a Co^{I} state (41).

To understand the propensity of ACS to undergo reversible methylation from CoFeSP, the relative nucleophilicity of a protein-ligated Ni^{I} center and a corrin-bound Co^{I} site toward methyl group transfer was probed using the M121A NiAz model. Methylcobinamide (MeCbi), a small-molecule analog of the native CoFeSP protein that has been shown to be effective for methyl transfer and acetyl-CoA synthesis in ACS (10), was used to recapitulate the base-off form of the corrinoid cofactor (42). Upon addition of MeCbi to $Ni^{I}Az$, Co^{I}binamide is generated, with concomitant formation of an equal amount of S = 1/2 Ni–CH_3 Az (*SI Appendix*, Fig. S1). The rate of methylation of M121A $Ni^{I}Az$ is comparable between the MeCbi and CH_3I methyl donors (*SI Appendix*, Fig. S2). However, when generated using the CH_3I donor, the S = 1/2 Ni–CH_3 Az species decays over the timescale of minutes (33), while the concentration of the S = 1/2 Ni–CH_3 Az species generated from MeCbi reaches a low but constant value after ∼5 min, suggesting an equilibrium is established. The relative concentrations of Co^{I} and Ni^{I} observed using optical and EPR spectroscopy indicate $K_{eq} \approx 0.01$, corresponding to a free energy difference (ΔG) of +2.7 kcal/mol between the two methylated species. While the directionality of methyl transfer is reversed in the native ACS–CoFeSP complex, where $K_{eq} \approx 2.3$ (9), this corresponds to only a slight change in free energy (ΔG = −0.49 kcal/mol for methylation of nickel in ACS; ΔΔG = +3.2 kcal/mol). The observation of direct, two-electron methyl transfer between biologically relevant model components supports the chemical competence of Ni^{I} for ACS catalysis.

Addition of Both ACS Substrates to Nickel Azurin Generates a Stable Nickel Acetyl Species. Reduction of the S = 1/2 Ni–CH_3 Az species results in an EPR-silent, S = 1 Ni^{II}–CH_3 state, which was characterized using optical, magnetic circular

dichroism, and X-ray spectroscopies (33). Electronic structure analysis of the Ni^{II}–CH_3 state suggests this species is ideally suited for further reactivity, with filled d_{xz} and d_{yz} orbitals of appropriate energy and geometry to achieve effective overlap with an incoming CO ligand (33, 36). We thus hypothesized that, like ACS, introducing both substrates to the NiAz model could induce carbon–carbon bond coupling to form an acetyl species. To probe this hypothesis, time-resolved optical spectra were measured after mixing CH_3I into M121A Ni^{I}Az, with subsequent CO addition at varying time points after initiating the reaction (Fig. 2*A*). Dramatic changes in the optical spectra and kinetics are observed upon introduction of CO. Using singular value decomposition (SVD) to analyze the spectra as a function of time and substrate concentrations, five distinct components are found to contribute to the overall spectra (*SI Appendix*, Fig. S3) (43). The spectral reconstruction of these components maps onto the previously observed spectra for Ni^{I}Az, S = 1/2 Ni–CH_3, S = 1 Ni^{II}–CH_3, and a new product species (*SI Appendix*, Fig. S3); depending on the time of CO addition, contributions from Ni^{I}–CO Az are also observed (*SI Appendix*, Fig. S4), reflecting the slower, weaker binding of CH_3I to Ni^{I}Az than CO. The new product spectrum is markedly distinct from the other species, with maxima at ∼345 and ∼415 nm and a substantial tail into the visible region of the spectrum. EPR spectra of analogous samples quenched at relevant time points show only the decrease of the S = 1/2 M121A Ni^{I}Az and Ni–CH_3 states, indicating that the new species is EPR silent (*SI Appendix*, Fig. S5).

Nickel K-edge X-ray absorption spectroscopy was performed for further characterization of this new species. An EPR-silent sample was generated upon sequential addition of CH_3I and CO to Ni^{I}Az (*SI Appendix*, Fig. S6), indicating complete conversion of the Ni–CH_3 Az species to the new product state. The extended X-ray absorption fine structure (EXAFS) region of the spectrum of the new species was best modeled with nickel contained in a four-coordinate environment with one nickel–sulfur scatterer at a distance of 2.27 Å and three nickel–light atom scatterers (C/N/O; modeled as nitrogen) at an average distance of 2.02 Å (Fig. 2*B* and *SI Appendix*, Table S1). An acceptable fit required the construction of phase and amplitude functions for

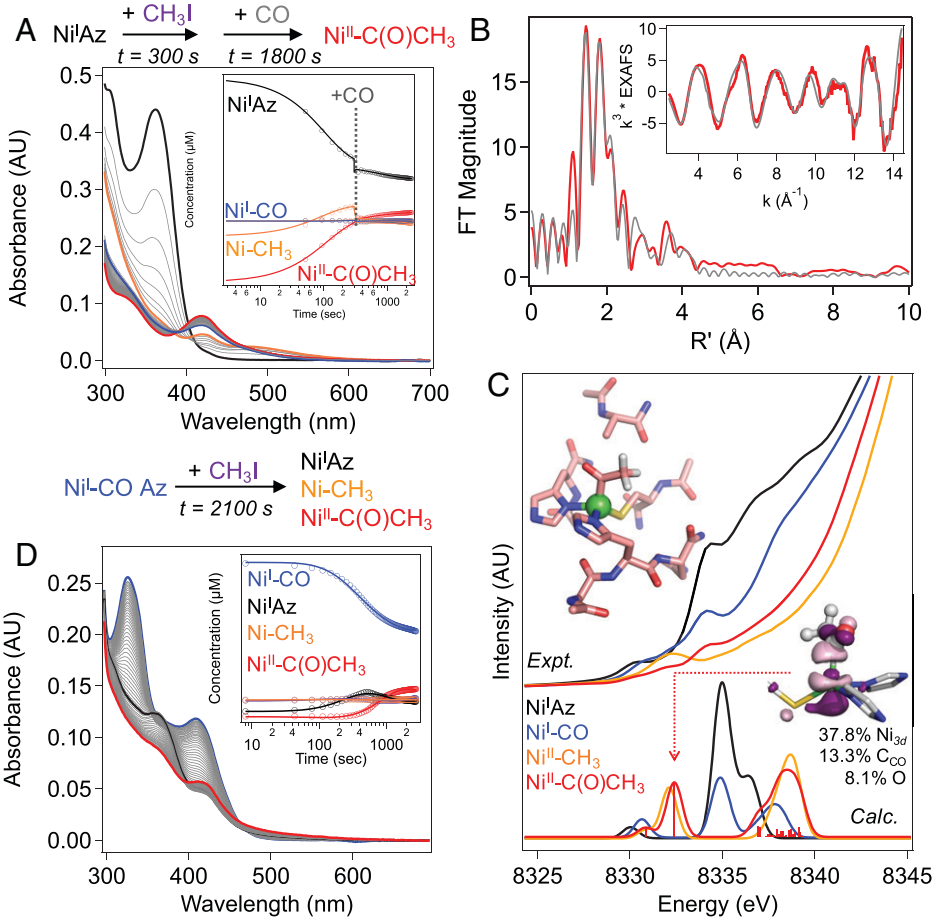

Fig. 2. Formation and characterization of a nickel acetyl Az species. (*A*) Optical spectra following rapid mixing of 5 mM CH_3I into 300 μM M121A Ni^{I}Az (black) in 50 mM phosphate, pH 8.0 (t = 0). At t = 300 s, CO-saturated buffer was added to a final concentration of 220 μM CO (blue), and spectra were collected each minute for 45 min (final trace shown in red). (*Inset*) Experimental SVD component amplitudes (open circles) overlaid with the global kinetic model (solid lines) for the reaction scheme shown in Fig. 4*A* with the rate constants given in *SI Appendix*, Fig. S3. Note that both the S = 1/2 and S = 1 Ni–CH_3 species contribute to the observed spectra and component traces shown in orange. (*B*) The non-phase-shift-corrected magnitude Fourier transform for Ni^{II}–C(O)CH_3 Az (red) overlaid with the best-fit simulation (gray). (*Inset*) Corresponding Ni K-edge k^3 EXAFS spectrum of Ni^{II}–C(O)CH_3 (red) overlaid with the best-fit simulation (gray). (*C*) Near-edge X-ray absorption spectra of 1 mM M121A Ni^{I}Az (black), Ni^{I}–CO Az (blue), Ni^{II}–CH_3 Az (orange), and Ni^{II}–C(O)CH_3 Az (red). Experimental spectra (*Top*) are compared to TD-DFT calculated spectra (*Bottom*; all offset by +7 eV) for geometry-optimized structures of each species. (*Top Inset*) DFT geometry-optimized structure of the Ni^{II}–C(O)CH_3 Az species. Hydrogen atoms other than those on the methyl group are omitted for clarity. (*Bottom Inset*) Singly occupied molecular orbital that gives rise to the preedge feature along with calculated atomic contributions to the molecular orbital. (*D*) Optical spectra following rapid mixing of 390 μM CH_3I into 190 μM M121A Ni^{I}–CO Az in 50 mM phosphate, pH 8.0. (*Inset*) Experimental SVD component amplitudes (open circles) overlaid with the global kinetic model (solid lines) for the reaction scheme shown in Fig. 4*A* with the rate constants given in *SI Appendix*, Fig. S17. Black trace highlights the characteristic optical feature of Ni^{I}Az at 364 nm appearing after addition of CH_3I to Ni^{I}–CO Az (blue trace).

two outer-sphere Ni-imidazole scattering pathways (33, 44–46). Although a statistically satisfactory solution to the EXAFS data was obtained by splitting the Ni–N and Ni–C scatterers into two shells, resulting in two Ni–N scatterers at 2.03 Å and one Ni–C scatterer at 1.97 Å, with corresponding outer-sphere imidazole scattering pathways, the resolution of the data does not warrant this separation. To obtain a structural model of this species, a spectroscopically validated, truncated fragment of M121A NiAz was used to represent the protein-bound active site, with an acetyl group added to the nickel center at the open axial coordination site (Fig. 2 *C*, *Top Inset*). The geometry could be optimized with the acetyl group bound to the Ni^{II} center in either a low-spin (S = 0) or a high-spin (S = 1) state, giving square planar or trigonal pyramidal structures, respectively. The energies of the two species differed by only 6 kcal/mol, which is within the error of the method and does not provide sufficient grounds for differentiation. However, the calculated structural metrics differ significantly. The calculated structural metrics of the S = 1 Ni^{II}–$C(O)CH_3$ Az species are in good agreement with the experimental parameters obtained from EXAFS analysis, while the bond lengths for the S = 0 state are calculated to be substantially shorter than those resolved experimentally (*SI Appendix*, Tables S1 and S2). The S = 0 Ni^{II}–$C(O)CH_3$ Az structural metrics are also in agreement with those observed for synthetic Ni^{II}-acyl species, suggesting the computational model would be chemically reasonable (47, 48). Further evidence in favor of the high-spin Ni^{II}-acetyl Az species is garnered by considering the steric clashes that would occur between the added acyl group and the backbone of the hydrophobic core of the protein in the low-spin configuration (*SI Appendix*, Fig. S7), along with the intensity of the optical transitions, which are characteristic of noncentrosymmetric charge transfer bands. While, to the best of our knowledge, there are no structurally characterized synthetic S = 1 Ni^{II}-acetyl species, we are also unaware of any previously isolated protein-bound nickel acyl species. Optimization with distinct CO and methyl ligands retained both imidazole ligands and the thiolate coordination (*SI Appendix*, Fig. S8), opposing the four-coordinate structure suggested by the EXAFS fits.

Analysis of the X-ray absorption near-edge structure (XANES) region of the spectrum provides additional insight into the electronic structure of the putative Ni^{II}-acetyl species (Fig. 2 *C*, *Top*). Relative to the Ni^{I}Az and Ni^{I}–CO Az species, which exhibit preedge features at 8,330.2 and 8,330.8 eV, respectively, the Ni^{II}–$C(O)CH_3$ species shows a preedge feature that is blue shifted to 8,332 eV (*SI Appendix*, Fig. S9). This feature occurs at a similar energy as the preedge transition in the previously characterized Ni^{II}–CH_3 Az species, although the new species exhibits decreased intensity relative to Ni^{II}–CH_3 Az. In addition, higher-energy transitions are also observed at positions similar to those in the Ni^{I}Az and Ni^{I}–CO Az species, likely due to mixing with charge transfer transitions (49, 50). The nature of these transitions was investigated using DFT calculations. Time-dependent DFT calculations of the core X-ray absorption transitions for Ni^{I}Az, Ni^{I}–CO Az, Ni^{II}–CH_3 Az, and Ni^{II}–$C(O)CH_3$ species reproduce the spectroscopic signatures, including the relative shifts in energy (Fig. 2 *C*, *Bottom*), allowing the dominant transition in the Ni^{II}–$C(O)CH_3$ species to be assigned to the population of a singly occupied molecular orbital with nickel–carbon antibonding character (Fig. 2 *C*, *Bottom Inset*). Collectively, the optical, EXAFS, XANES, and DFT studies suggest the formation of an S = 1 Ni^{II}–$C(O)CH_3$ species in M121A NiAz upon the addition of the one-carbon precursors, CO and CH_3I, analogous to the carbon–carbon bond-forming reaction that occurs in ACS.

Distinct kinetics and spectral signatures were observed when starting from the Ni^{I}–CO state. Time-resolved optical spectra reveal that, upon addition of CH_3I to M121A Ni^{I}–CO Az, the Ni^{I}–CO state decays to the Ni^{I}Az state. This conversion precedes generation of the absorption features that are characteristic of the S = 1/2 Ni–CH_3 Az and S = 1 Ni^{II}–CH_3 species (Fig. 2*D* and *SI Appendix*, Fig. S17). Rapid-freeze-quench EPR spectroscopy also shows the appearance of Ni^{I}Az along with formation of the S = 1/2 Ni–CH_3 state (*SI Appendix*, Figs. S12 and S13). Unlike the EPR-silent species formed upon addition of CO to the Ni–CH_3 species, XAS spectra of a sample prepared by addition of CH_3I to M121A Ni^{I}–CO Az show a mixture of components, including evidence for the Ni^{I}Az, Ni^{I}–CO Az, and Ni–CH_3 species along with the Ni^{II}-acetyl species (*SI Appendix*, Figs. S10 and S11) (51).

The time-resolved optical and EPR spectra were modeled using quantitative kinetic analyses across a range of conditions to obtain a self-consistent mechanism for formation of the nickel acetyl species starting from the Ni^{I}–CO Az state. A series of rapid-mixing experiments were used to extract the rate constants for CO binding and dissociation to Ni^{I}Az, which are estimated at ∼400 $M^{-1}{\cdot}s^{-1}$ and 0.06 s^{-1}, respectively (*SI Appendix*, Figs. S14–S16), in the absence of any additional substrates. In native ACS, these rate constants are modeled to be greater, with CO binding occurring with a rate constant of $\sim10^4$ $M^{-1}{\cdot}s^{-1}$ to 10^6 $M^{-1}{\cdot}s^{-1}$ and CO dissociation estimated between 9.1 s^{-1} and 64.8 s^{-1} (8, 41). SVD of the optical spectra following addition of CH_3I to Ni^{I}–CO reveals component spectra that represent the Ni^{I}Az, Ni^{I}–CO, S = 1/2 Ni–CH_3, Ni^{II}–CH_3, and Ni^{II}–$C(O)CH_3$ species. Substantial amounts of the species corresponding to Ni^{I}Az are observed prior to the formation of the S = 1/2 Ni–CH_3 species, suggesting dissociation of CO prior to methyl binding in an ordered pathway. Consistent with this hypothesis, quantitative kinetic modeling of a series of complementary rapid-mixing optical and EPR experiments indicates that the spectra are most accurately reconstructed if the rate of direct methyl addition to the Ni^{I}–CO Az state is zero (*SI Appendix*, Figs. S17 and S18). Forcing a nonzero rate necessitates substantially slower CO dissociation rates than observed in the other experiments, gives a much higher CO binding affinity than experimentally observed, and converges on a methyl insertion rate into Ni^{I}-CO that is approximately an order of magnitude lower than CO insertion into the Ni–CH_3 species (*SI Appendix*, Fig. S19). Collectively, these data favor a sequential, ordered pathway for nickel acetyl formation from the Ni^{II}–CH_3 state, although a slow, parallel pathway cannot be excluded.

Chemical Quenching of Nickel Acetyl Azurin Releases Acetic Acid. In the absence of CoA, the native ACS enzyme is suggested to accumulate a protein-bound Ni^{II}-acetyl group that slowly hydrolyzes to release acetate (5, 7, 52). However, this state has only been inferred on the basis of rapid reaction of the isolated protein with CoA to release stoichiometric amounts of acetyl CoA (8, 10, 41), as well as the rapid exchange between isotopically labeled CoA and acetyl-CoA relative to exchange with solution-phase CO (53–55). To assess the capacity of the designed M121A NiAz system to effect analogous chemistry from the Ni^{II}-acetyl state, assays were performed in which M121A Ni^{I}Az was allowed to react with $^{13}CH_3I$ for a fixed amount of time prior to introducing CO into the system. Reactions were quenched by the addition of perchloric acid to hydrolyze the putative metal–acyl species and precipitate the protein, and ^{13}C NMR spectroscopy was used to analyze the

products in conjunction with an internal quantification standard (*SI Appendix*, Fig. S20). When both $^{13}CH_3I$ and CO are added to M121A $Ni^{I}Az$, a new peak is observed at 20.4 ppm in the ^{13}C NMR spectrum that corresponds to the methyl carbon of ^{13}C-labeled acetic acid (Fig. 3*A*), with a yield of 20 to 40% relative to the initial $Ni^{I}Az$ concentration. An additional 300-Hz splitting is observed when ^{13}CO is used, indicating that both exogenously added substrates are incorporated into the acetic acid product, and a similarly split peak is observed that corresponds to the carbonyl carbon. No new features are observed in the absence of either substrate, without M121A $Ni^{I}Az$, or using either M121A $Cu^{I}Az$, M121A apo-Az, or free Ni^{II}, confirming that the acetic acid product is generated by the specific reaction of M121A $Ni^{I}Az$ with CO and CH_3I (*SI Appendix*, Fig. S21).

Mechanistic insight was obtained by investigating the amount of acetic acid formed under different reaction conditions. Mimicking the reported conditions for ACS activity assays, the M121A NiAz reaction assays were typically performed in the presence of Ti^{III}(citrate) to maintain a low solution reduction potential. The presence of reductant was found to directly impact the amount of acetic acid formed; in the absence of any exogenous reducing agent, no acetic acid is observed, with increasing amounts observed as the concentration of Ti^{III}(citrate) rises (*SI Appendix*, Fig. S22). That an added electron is needed for product formation, in line with the absence of any new EPR-active species observed over the course of the reaction, suggests that acetyl formation occurs from an EPR-silent Ni^{II} state of the protein rather than the $S = 1/2$ Ni–CH_3 state. The amount of CH_3I added had little effect on acetic acid yield, provided the concentrations were in large excess relative to M121A $Ni^{I}Az$, and the yields were only moderately sensitive to the time after reaction at which CO was added to the Ni–CH_3 species, with the greatest yields obtained upon concerted substrate addition (*SI Appendix*, Fig. S22 and Table S3).

Addition of $^{13}CH_3I$ to M121A Ni^{I}–CO Az and subsequent acid quenching and extraction results in the generation of comparable amounts of acetic acid, with doubly ^{13}C-labeled product observed when starting from Ni^{I}–^{13}CO Az (*SI Appendix*, Fig. S23). As seen in the optical spectra, these reactions also proceed through the formation of $Ni^{I}Az$ (*SI Appendix*, Fig. S24). Small (<5%) amounts of ^{13}C-labeled acetone were also observed when initiating the reaction from the Ni^{I}–CO state (*SI Appendix*, Figs. S25 and S26). This interesting side reaction appears to occur predominantly when starting from the Ni^{I}–CO state and in the presence of excess CH_3I; removal of excess CH_3I prior to reaction with CO suppresses acetone formation (*SI Appendix*, Table S3). In native ACS, the conformational gating that controls binding of the CoFeSP protein and methyl transfer would preclude superstoichiometric methyl addition (56), preventing this unproductive process.

Thiol Addition to Nickel Acetyl Azurin Yields an Activated Thioester. The electronic structure characterization of M121A Ni^{II}-acetyl Az reveals an electrophilic acyl carbon (*SI Appendix*, Table S4), consistent with the propensity for hydrolysis upon acidification. Given the potential lability of the metal–acyl bond, we were interested in investigating whether acyl release could be promoted through C–S bond formation, resulting in an activated thioester analogous to acetyl-CoA. Indeed, using NMR analysis, S-methylthioacetate was detected at 29.76 ppm in large quantities upon addition of S-methylthiolate to the reaction following both $^{13}CH_3I$ and CO addition to M121A $Ni^{I}Az$ (Fig. 3*B*), indicating that this model protein reproduces the thioester synthesis reaction of ACS from C_1 precursors. The S-methylthioacetate product was quantified in up to 70% yield relative to NiAz, with no detectable product in any of the relevant control experiments (*SI Appendix*, Figs. S27 and S28). Intact reaction mixtures were analyzed within 4 h to minimize hydrolysis of the thioester, which, while slow in neutral water (57), occurs rapidly in the presence of the protein and other

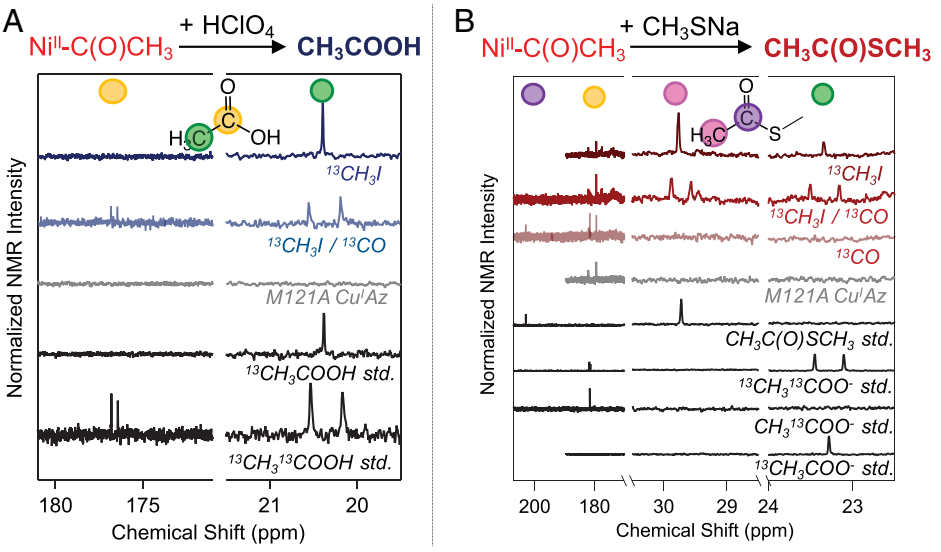

Fig. 3. Product formation from M121A NiAz upon ACS substrate addition. (*A*) Semiquantitative ^{13}C NMR spectra showing acetic acid formation from acid-quenched reactions of M121A Ni-CH_3 Az + 1 atm CO in the presence of 5 mM Ti^{III}citrate with the indicated isotopic labels. Also shown are control traces for analogous reactions performed with M121A $Cu^{I}Az$ (gray) and acetic acid standards (black). The reactions and standards were run in 50 mM D_2O phosphate buffer (initial pD 7.6) in the presence of 30 mM DSS internal standard and 500 mM perchloric acid. (*B*) Semiquantitative ^{13}C NMR spectra showing thioester formation from reactions of 1 mM M121A $Ni^{I}Az$ with 25 mM CH_3I and 1 atm CO in the presence of 5 mM Ti^{III}citrate with the indicated isotopic labels; 50 mM CH_3SNa was added sequentially as the third substrate in all reactions. Also shown are control traces for analogous reactions performed with M121A $Cu^{I}Az$ (gray), 25 mM S-methylthioacetate (black), and acetic acid standards (black). Reactions and standards were run in 50 mM phosphate in D_2O, pD 7.6, in the presence of 30 mM DSS.

reactants (*SI Appendix*, Fig. S29). Use of ^{13}CO resulted in an additional 192-Hz splitting of the methyl peak, while performing the reaction with $^{NA}CH_3I$ and ^{13}CO showed a carbonyl peak at 202 ppm, exactly aligned with the S-methylthioacetate standard sample. In addition to S-methylthioacetate, acetate was observed in only ∼10 to 20% yields, and small amounts of acetone were observed in some samples. Similar to NiAz, acetate has also been reported in up to 20% yields as a side reaction in native ACS, independent of the presence of CoA (52, 58). As in the acid-quenched samples, thioester product is only observed in the presence of exogenous reductant, although small amounts of acetate are observed in the absence of Ti^{III}(citrate), possibly from intermolecular reduction (*SI Appendix*, Fig. S30 and Table S3). The product distribution is largely unchanged when starting from the Ni^{I}–CO state and adding $^{13}CH_3I$ followed by S-methylthiolate (*SI Appendix*, Fig. S31), consistent with a common mechanism, although the largest amounts of thioester are produced when CH_3I is the first substrate or both substrates are added concurrently (*SI Appendix*, Table S3). The relative proportions of thioester to acetate observed indicate that the rate of thiolysis is at least twofold faster than the rate of hydrolysis. To correlate the optical signals observed upon rapid mixing with the two-carbon products generated, the protein has been isolated and concentrated following addition of both CH_3I and CO to dilute solutions of Ni^{I}Az. In these samples, the optical spectra remain unchanged upon concentration (*SI Appendix*, Figs. S24 and S32), consistent with the generation of a stable Ni^{II}–$C(O)CH_3$ state, and addition of methylthiolate to the NMR samples results in thioester formation with no evidence of acetate production (*SI Appendix*, Fig. S24). Across all conditions, up to near-stoichiometric amounts of thioester are produced relative to NiAz under substrate- and reductant- replete conditions, highlighting the selectivity of the model protein system toward thiolysis over hydrolysis.

Discussion

Drawing on the observed reactivity of M121A NiAz as a well-defined biochemical model with chemical capability analogous to ACS, we propose a modified reaction mechanism for both systems (Fig. 4). While either isolated substrate can bind to the M121A Ni^{I}Az active site, the CO-bound metal center is not competent for subsequent rapid methyl binding. Instead, the kinetically preferred pathway indicates that CO dissociates prior to methyl addition. This sequence is consistent with the reactivity observed in synthetic compounds; the addition of an alkyl group to a Ni^{I}–CO complex is only seen to proceed via one-electron, radical transformations (47, 59–61). One-electron reduction of the S = 1/2 Ni–CH_3 species to the S = 1 Ni^{II}–CH_3 Az state must precede CO addition to the nickel center, as no new EPR-active species are observed when CO is added to the S = 1/2 Ni–CH_3 Az species. Product formation is also seen to require the presence of reductant (*SI Appendix*, Figs. S22 and S30). CO binding gives a transient Ni(CO)(CH_3) state that undergoes spontaneous methyl migration or CO insertion to form a stable nickel acetyl species, which is suggested, from the spectroscopic data, to have an S = 1 spin state. Rapid thiolysis or slower hydrolysis of the M121A Ni^{II}-acetyl Az species releases thioester or acetate with concomitant generation of a Ni^{0} center. A cyclic process to regenerate the chemically competent Ni^{I}Az species under the current conditions is feasible. The requisite reduction of the S = 1/2 Ni–CH_3 Az species to the S = 1 Ni^{II}–CH_3 Az species by Ti^{III}(citrate) generates Ti^{IV}(citrate), which could serve as an electron acceptor. However, only stoichiometric amounts of Ti^{IV}(citrate) are produced, and Ti^{IV}(citrate) can easily hydrolyze to generate inert, insoluble TiO_2, rendering it a poor candidate as a solution-phase oxidant. Instead, upon thiolysis, the resultant Ni^{0} is likely released from the protein; in support of this hypothesis, attempts to optimize a Ni^{0}Az species in silico resulted in a highly energetic structure with complete loss of His46 coordination (*SI Appendix*, Fig. S33). To enable multiple turnovers, we suggest that functionally reproducing the [4Fe-4S] cluster in ACS will be critical, enabling regeneration of the Ni^{I}Az state and thus a catalytic process.

In native ACS, this electron may come from the [4Fe-4S] subsite of the A-cluster. While the cluster has been proposed to be inert to electron transfer on the basis of experiments performed on nickel-depleted subunits of the enzyme (62), the redox properties are likely to differ dramatically when the cofactor is properly assembled within the full protein complex (63). Thus, we suggest that the cluster functions as a storage site for an electron, with a reduction potential that is matched to the reduction of the S= 1/2 Ni–CH_3 state. In ACS, thiolysis by CoA would reduce the [4Fe-4S] cluster to regenerate the catalytically competent Ni^{I} state.

The mechanistic information provided by the M121A NiAz model protein provides insight into the workings of the native ACS enzyme. The observation that the M121A NiAz system, with only a single nickel center, is capable of carrying out the reactions performed by ACS with reasonable yields has

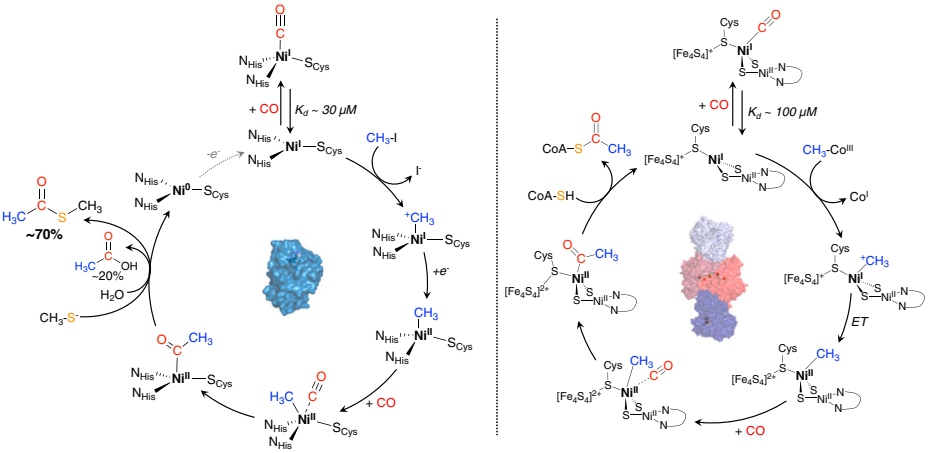

Fig. 4. Proposed mechanisms for thioester synthesis by M121A NiAz (*Left*) and ACS (*Right*).

implications for the evolution of the enzyme, suggesting that a multimetallic center is not critical for activity. Instead, we postulate that the Ni_D center may control the geometric and electronic structure of the Ni_P site, preventing disulfide formation, constraining the metal ligation, and reducing the nucleophilicity of the cysteine thiolates to avoid alkylation. In this way, the two histidine residues in NiAz may serve a role similar to the bridging Cys595 and Cys597 (*Mt* numbering) residues in ACS (64–67), as similar geometric parameters are observed (*SI Appendix*, Table S5), and the nucleophilicity of a histidine ligand is likely to be comparable to that of a bridging thiolate (67, 68). By constructing a functional model of ACS within a simplified protein platform, the minimal requirements for activity have been established. This work presents an opportunity for further elucidation of structure–function correlations within the native enzyme and model systems, expanding the potential link between abiotic chemistry and the complex biological metabolic processes that are ubiquitous today.

Data Availability. All study data are included in the article and/or *SI Appendix*.

ACKNOWLEDGMENTS. We gratefully acknowledge Professor David Grahame (Uniformed Services University of the Health Sciences) for the generous donation of methylcobinamide and Professor Yi Lu (University of Texas at Austin) for providing the M121A Az plasmid. We thank Dr. Tanya Whitmer (The Ohio State University) for assistance with NMR measurements and Professor Patrick Holland (Yale University) for helpful discussions. Funding was provided by US Department of Energy Basic Energy Sciences Grant DE-SC0018020 to H.S.S. Also, J.S. acknowledges the NIH for support (Grant R15-GM141650). X-ray absorption spectroscopic studies were performed at the Canadian Light Source, a national research facility of the University of Saskatchewan, which is supported by the Canada Foundation for Innovation, the Natural Sciences and Engineering Research Council, the National Research Council, the Canadian Institutes of Health Research, the Government of Saskatchewan, and the University of Saskatchewan.

Author affiliations: [a]The Ohio State Biochemistry Program, The Ohio State University, Columbus, OH 43210; [b]Department of Chemistry, Trinity University, San Antonio, TX 78212; and [c]Department of Chemistry and Biochemistry, The Ohio State University, Columbus, OH 43210

1. C. Huber, G. Wächtershäuser, Activated acetic acid by carbon fixation on (Fe,Ni)S under primordial conditions. *Science* **276**, 245–247 (1997).
2. C. Huber, W. Eisenreich, S. Hecht, G. Wächtershäuser, A possible primordial peptide cycle. *Science* **301**, 938–940 (2003).
3. M. C. Weiss *et al.*, The physiology and habitat of the last universal common ancestor. *Nat. Microbiol.* **1**, 16116 (2016).
4. P. S. Adam, G. Borrel, S. Gribaldo, Evolutionary history of carbon monoxide dehydrogenase/acetyl-CoA synthase, one of the oldest enzymatic complexes. *Proc. Natl. Acad. Sci. U.S.A.* **115**, E1166–E1173 (2018).
5. S. W. Ragsdale, H. G. Wood, Acetate biosynthesis by acetogenic bacteria. Evidence that carbon monoxide dehydrogenase is the condensing enzyme that catalyzes the final steps of the synthesis. *J. Biol. Chem.* **260**, 3970–3977 (1985).
6. M. Can, F. A. Armstrong, S. W. Ragsdale, Structure, function, and mechanism of the nickel metalloenzymes, CO dehydrogenase, and acetyl-CoA synthase. *Chem. Rev.* **114**, 4149–4174 (2014).
7. T. I. Doukov, T. M. Iverson, J. Seravalli, S. W. Ragsdale, C. L. Drennan, A Ni-Fe-Cu center in a bifunctional carbon monoxide dehydrogenase/acetyl-CoA synthase. *Science* **298**, 567–572 (2002).
8. X. Tan, I. V. Surovtsev, P. A. Lindahl, Kinetics of CO insertion and acetyl group transfer steps, and a model of the acetyl-CoA synthase catalytic mechanism. *J. Am. Chem. Soc.* **128**, 12331–12338 (2006).
9. X. S. Tan, C. Sewell, P. A. Lindahl, Stopped-flow kinetics of methyl group transfer between the corrinoid-iron-sulfur protein and acetyl-coenzyme A synthase from *Clostridium thermoaceticum*. *J. Am. Chem. Soc.* **124**, 6277–6284 (2002).
10. S. Gencic, D. A. Grahame, Two separate one-electron steps in the reductive activation of the A cluster in subunit β of the ACDS complex in *Methanosarcina thermophila*. *Biochemistry* **47**, 5544–5555 (2008).
11. J. Seravalli, S. W. Ragsdale, Pulse-chase studies of the synthesis of acetyl-CoA by carbon monoxide dehydrogenase/acetyl-CoA synthase: Evidence for a random mechanism of methyl and carbonyl addition. *J. Biol. Chem.* **283**, 8384–8394 (2008).
12. S. J. George, J. Seravalli, S. W. Ragsdale, EPR and infrared spectroscopic evidence that a kinetically competent paramagnetic intermediate is formed when acetyl-coenzyme A synthase reacts with CO. *J. Am. Chem. Soc.* **127**, 13500–13501 (2005).
13. P. A. Lindahl, Acetyl-coenzyme A synthase: The case for a Ni(p)(0)-based mechanism of catalysis. *J. Biol. Inorg. Chem.* **9**, 516–524 (2004).
14. R. P. Schenker, T. C. Brunold, Computational studies on the A cluster of acetyl-coenzyme A synthase: Geometric and electronic properties of the NiFeC species and mechanistic implications. *J. Am. Chem. Soc.* **125**, 13962–13963 (2003).
15. S. W. Ragsdale, "Biological carbon fixation by an organometallic pathway: Evidence supporting the paramagnetic mechanism of the nickel-iron-sulfur acetyl-CoA synthase" in *Comprehensive Coordination Chemistry III*, E. Constable, G. Parkin, L. Que, Eds. (Elsevier, 2021), pp. 611–633.
16. S. E. Cohen *et al.*, Crystallographic characterization of the carbonylated A-cluster in carbon monoxide dehydrogenase/acetyl-CoA synthase. *ACS Catal.* **10**, 9741–9746 (2020).
17. M. Can, L. J. Giles, S. W. Ragsdale, R. Sarangi, X-ray absorption spectroscopy reveals an organometallic Ni-C bond in the CO-treated form of acetyl-CoA synthase. *Biochemistry* **56**, 1248–1260 (2017).
18. C. D. James, S. Wiley, S. W. Ragsdale, B. M. Hoffman, ^{13}C electron nuclear double resonance spectroscopy shows acetyl-CoA synthase binds two substrate CO in multiple binding modes and reveals the importance of a CO-binding "alcove." *J. Am. Chem. Soc.* **142**, 15362–15370 (2020).
19. P. Stavropoulos, M. C. Muetterties, M. Carrie, R. H. Holm, Structural and reaction chemistry of nickel complexes in relation to carbon monoxide dehydrogenase: A reaction system simulating acetyl-coenzyme A synthase activity. *J. Am. Chem. Soc.* **113**, 8485–8492 (1991).
20. W. G. Dougherty, K. Rangan, M. J. O'Hagan, G. P. A. Yap, C. G. Riordan, Binuclear complexes containing a methylnickel moiety: Relevance to organonickel intermediates in acetyl coenzyme A synthase catalysis. *J. Am. Chem. Soc.* **130**, 13510–13511 (2008).
21. P. W. G. Ariyananda, M. T. Kieber-Emmons, G. P. A. Yap, C. G. Riordan, Synthetic analogs for evaluating the influence of N-H...S hydrogen bonds on the formation of thioester in acetyl coenzyme A synthase. *Dalton Trans.* **2009**, 4359–4369 (2009).
22. M. Ito, M. Kotera, T. Matsumoto, K. Tatsumi, Dinuclear nickel complexes modeling the structure and function of the acetyl CoA synthase active site. *Proc. Natl. Acad. Sci. U.S.A.* **106**, 11862–11866 (2009).
23. G. C. Tucci, R. H. Holm, Nickel-mediated formation of thio esters from bound methyl, thiols, and carbon monoxide: A possible reaction pathway of acetyl-coenzyme A synthase activity in nickel-containing carbon monoxide dehydrogenases. *J. Am. Chem. Soc.* **117**, 6489–6496 (1995).
24. M. Hay, J. H. Richards, Y. Lu, Construction and characterization of an azurin analog for the purple copper site in cytochrome c oxidase. *Proc. Natl. Acad. Sci. U.S.A.* **93**, 461–464 (1996).
25. A. Bhagi-Damodaran *et al.*, Why copper is preferred over iron for oxygen activation and reduction in haem-copper oxidases. *Nat. Chem.* **9**, 257–263 (2017).
26. J. W. Slater, S. C. Marguet, H. A. Monaco, H. S. Shafaat, Going beyond structure: Nickel-substituted rubredoxin as a mechanistic model for the [NiFe] hydrogenases. *J. Am. Chem. Soc.* **140**, 10250–10262 (2018).
27. Y. Yu *et al.*, A designed metalloenzyme achieving the catalytic rate of a native enzyme. *J. Am. Chem. Soc.* **137**, 11570–11573 (2015).
28. J. D. Caranto, A. C. Vilbert, K. M. Lancaster, *Nitrosomonas europaea* cytochrome P460 is a direct link between nitrification and nitrous oxide emission. *Proc. Natl. Acad. Sci. U.S.A.* **113**, 14704–14709 (2016).
29. C. Esmieu, P. Raleiras, G. Berggren, From protein engineering to artificial enzymes - Biological and biomimetic approaches towards sustainable hydrogen production. *Sustain. Energy Fuels* **2**, 724–750 (2018).
30. J. J. Warren, K. M. Lancaster, J. H. Richards, H. B. Gray, Inner- and outer-sphere metal coordination in blue copper proteins. *J. Inorg. Biochem.* **115**, 119–126 (2012).
31. N. Bonander, B. G. Karlsson, T. Vänngård, Environment of copper in *Pseudomonas aeruginosa* azurin probed by binding of exogenous ligands to Met121X (X = Gly, Ala, Val, Leu, or Asp) mutants. *Biochemistry* **35**, 2429–2436 (1996).
32. A. C. Manesis, M. J. O'Connor, C. R. Schneider, H. S. Shafaat, Multielectron chemistry within a model nickel metalloprotein: Mechanistic implications for acetyl-CoA synthase. *J. Am. Chem. Soc.* **139**, 10328–10338 (2017).
33. A. C. Manesis *et al.*, A biochemical nickel(I) state supports nucleophilic alkyl addition: A roadmap for methyl reactivity in acetyl coenzyme A synthase. *Inorg. Chem.* **58**, 8969–8982 (2019).
34. G. Bender *et al.*, Infrared and EPR spectroscopic characterization of a Ni(I) species formed by photolysis of a catalytically competent Ni(I)-CO intermediate in the acetyl-CoA synthase reaction. *Biochemistry* **49**, 7516–7523 (2010).
35. A. C. Manesis, H. S. Shafaat, Electrochemical, spectroscopic, and density functional theory characterization of redox activity in nickel-substituted azurin: A model for acetyl-CoA synthase. *Inorg. Chem.* **54**, 7959–7967 (2015).
36. E. C. Kisgeropoulos, A. C. Manesis, H. S. Shafaat, Ligand field inversion as a mechanism to gate bioorganometallic reactivity: Investigating a biochemical model of acetyl CoA synthase using spectroscopy and computation. *J. Am. Chem. Soc.* **143**, 849–867 (2021).
37. R. Hoffmann *et al.*, From widely accepted concepts in coordination chemistry to inverted ligand fields. *Chem. Rev.* **116**, 8173–8192 (2016).
38. Y. M. Hsiao, S. S. Chojnacki, P. Hinton, J. H. Reibenspies, M. Y. Darensbourg, Organometallic chemistry of sulfur/phosphorus donor ligand complexes of nickel(II) and nickel(0). *Organometallics* **12**, 870–875 (1993).
39. M. S. Oderinde, M. Frenette, D. W. Robbins, B. Aquila, J. W. Johannes, Photoredox mediated nickel catalyzed cross-coupling of thiols with aryl and heteroaryl iodides via thiyl radicals. *J. Am. Chem. Soc.* **138**, 1760–1763 (2016).
40. Y. Qin, R. Sun, N. P. Gianoulis, D. G. Nocera, Photoredox nickel-catalyzed C–S cross-coupling: Mechanism, kinetics, and generalization. *J. Am. Chem. Soc.* **143**, 2005–2015 (2021).
41. J. Seravalli, M. Kumar, S. W. Ragsdale, Rapid kinetic studies of acetyl-CoA synthesis: Evidence supporting the catalytic intermediacy of a paramagnetic NiFeC species in the autotrophic Wood-Ljungdahl pathway. *Biochemistry* **41**, 1807–1819 (2002).
42. T. Svetlitchnaia, V. Svetlitchnyi, O. Meyer, H. Dobbek, Structural insights into methyltransfer reactions of a corrinoid iron–sulfur protein involved in acetyl-CoA synthesis. *Proc. Natl. Acad. Sci. U.S.A.* **103**, 14331–14336 (2006).
43. K. A. Johnson, "Fitting enzyme kinetic data with KinTek Global Kinetic Explorer" in *Methods in Enzymology*, M. L. Johnson, L. Brand, Eds. (Academic, 2009), vol. **467**, pp 601–626.
44. R. C. Scarrow *et al.*, X-ray spectroscopy of nitrile hydratase at pH 7 and 9. *Biochemistry* **35**, 10078–10088 (1996).
45. J. Shearer, P. Soh, The copper(II) adduct of the unstructured region of the amyloidogenic fragment derived from the human prion protein is redox-active at physiological pH. *Inorg. Chem.* **46**, 710–719 (2007).

46. J. Shearer, K. L. Peck, J. C. Schmitt, K. P. Neupane, Cysteinate protonation and water hydrogen bonding at the active-site of a nickel superoxide dismutase metallopeptide-based mimic: Implications for the mechanism of superoxide reduction. *J. Am. Chem. Soc.* **136**, 16009–16022 (2014).
47. C. Yoo, S. Oh, J. Kim, Y. Lee, Transmethylation of a four-coordinate nickel(I) monocarbonyl species with methyl iodide. *Chem. Sci. (Camb.)* **5**, 3853–3858 (2014).
48. B. Horn, C. Limberg, C. Herwig, S. Mebs, The conversion of nickel-bound CO into an acetyl thioester: Organometallic chemistry relevant to the acetyl coenzyme A synthase active site. *Angew. Chem. Int. Ed. Engl.* **50**, 12621–12625 (2011).
49. I. M. DiMucci, S. N. MacMillan, R. C. Walroth, K. M. Lancaster, Scrutinizing "ligand bands" via polarized single-crystal X-ray absorption spectra of copper(I) and copper(II) bis-2,2′-bipyridine species. *Inorg. Chem.* **59**, 13416–13426 (2020).
50. T. Hatsui, Y. Takata, N. Kosugi, Strong metal-to-ligand charge transfer bands observed in Ni K- and L-edge XANES of planar Ni complexes. *J. Synchrotron Radiat.* **6**, 376–378 (1999).
51. S. Stoll, A. Schweiger, EasySpin, a comprehensive software package for spectral simulation and analysis in EPR. *J. Magn. Reson.* **178**, 42–55 (2006).
52. D. P. Barondeau, P. A. Lindahl, Methylation of carbon monoxide dehydrogenase from *Clostridium thermoaceticum* and mechanism of acetyl coenzyme A synthesis. *J. Am. Chem. Soc.* **119**, 3959–3970 (1997).
53. W. P. Lu, S. W. Ragsdale, Reductive activation of the coenzyme A/acetyl-CoA isotopic exchange reaction catalyzed by carbon monoxide dehydrogenase from *Clostridium thermoaceticum* and its inhibition by nitrous oxide and carbon monoxide. *J. Biol. Chem.* **266**, 3554–3564 (1991).
54. S. E. Ramer, S. A. Raybuck, W. H. Orme-Johnson, C. T. Walsh, Kinetic characterization of the [3′-32P]coenzyme A/acetyl coenzyme A exchange catalyzed by a three-subunit form of the carbon monoxide dehydrogenase/acetyl-CoA synthase from Clostridium thermoaceticum. *Biochemistry* **28**, 4675–4680 (1989).
55. B. Bhaskar, E. DeMoll, D. A. Grahame, Redox-dependent acetyl transfer partial reaction of the acetyl-CoA decarbonylase/synthase complex: Kinetics and mechanism. *Biochemistry* **37**, 14491–14499 (1998).
56. S. E. Cohen *et al.*, Negative-stain electron microscopy reveals dramatic structural rearrangements in Ni-Fe-S-dependent carbon monoxide dehydrogenase/acetyl-CoA synthase. *Structure* **29**, 43–49 (2021).
57. P. J. Bracher, P. W. Snyder, B. R. Bohall, G. M. Whitesides, The relative rates of thiol-thioester exchange and hydrolysis for alkyl and aryl thioalkanoates in water. *Orig. Life Evol. Biosph.* **41**, 399–412 (2011).
58. W. P. Lu, S. R. Harder, S. W. Ragsdale, Controlled potential enzymology of methyl transfer reactions involved in acetyl-CoA synthesis by CO dehydrogenase and the corrinoid/iron-sulfur protein from *Clostridium thermoaceticum*. *J. Biol. Chem.* **265**, 3124–3133 (1990).
59. C. Yoo, M. J. Ajitha, Y. Jung, Y. Lee, Mechanistic study on C–C bond formation of a nickel(I) monocarbonyl species with alkyl iodides: Experimental and computational investigations. *Organometallics* **34**, 4305–4311 (2015).
60. C. A. Laskowski *et al.*, Synthesis and reactivity of two-coordinate Ni(I) alkyl and aryl complexes. *J. Am. Chem. Soc.* **135**, 18272–18275 (2013).
61. E. E. Marlier, S. J. Tereniak, K. Ding, J. E. Milliken, C. C. Lu, First-row transition-metal chloride complexes of the wide bite-angle diphosphine (iPr)DPDBFphos and reactivity studies of monovalent nickel. *Inorg. Chem.* **50**, 9290–9299 (2011).
62. X. Tan, M. Martinho, A. Stubna, P. A. Lindahl, E. Münck, Mossbauer evidence for an exchange-coupled [Fe4S4]1+ Nip1+ A-cluster in isolated α subunits of acetyl-coenzyme A synthase/carbon monoxide dehydrogenase. *J. Am. Chem. Soc.* **130**, 6712–6713 (2008).
63. Y. Hu *et al.*, Nitrogenase reactivity with P-cluster variants. *Proc. Natl. Acad. Sci. U.S.A.* **102**, 13825–13830 (2005).
64. D. C. Fox, A. T. Fiedler, H. L. Halfen, T. C. Brunold, J. A. Halfen, Electronic structure control of the nucleophilicity of transition metal-thiolate complexes: An experimental and theoretical study. *J. Am. Chem. Soc.* **126**, 7627–7638 (2004).
65. J. N. Smith, Z. Shirin, C. J. Carrano, Control of thiolate nucleophilicity and specificity in zinc metalloproteins by hydrogen bonding: Lessons from model compound studies. *J. Am. Chem. Soc.* **125**, 868–869 (2003).
66. E. Almaraz *et al.*, Thiolate bridging and metal exchange in adducts of a zinc finger model and Pt(II) complexes: Biomimetic studies of protein/Pt/DNA interactions. *J. Am. Chem. Soc.* **130**, 6272–6280 (2008).
67. G. Ohanessian, D. Picot, G. Frison, Reactivity of polynuclear zinc-thiolate sites. *Int. J. Quantum Chem.* **111**, 1239–1247 (2011).
68. F. Brotzel, H. Mayr, Nucleophilicities of amino acids and peptides. *Org. Biomol. Chem.* **5**, 3814–3820 (2007).